Article ID: 1000-7032(2025)10-1851-11

Time-resolved Electroluminescence of Charge Carrier Dynamics in Multiple-emitting-layer White QLEDs with Polyethyleneimine Interlayers

YAN Shanshan[1], WANG Shen[1], LIANG Wencheng[1], LIU Weiwei[2*], KONG Youchao[2*]

(1. *College of Chemical and Material Engineering, Quzhou University, Quzhou* 324000, *China*;
2. *Department of Physics and Electronic Engineering, Yancheng Teachers University, Yancheng* 224002, *China*)

* *Corresponding Authors, E-mail: liuww@yctu. edu. cn; yb*87816*@um. edu. mo*

Abstract: The charge carrier transport and recombination dynamics in the quantum dots-based light-emitting diodes (QLEDs) featuring multiple emitting layers (M-EMLs) has a great impact on the device performance. In this work, QLEDs based on M-EMLs separated by polyethyleneimine ethoxylated (PEIE) layer with different stacking sequences of blue (B), green (G), and red (R) QDs layer were used to intuitively explore the injection, transportation and recombination processes of the charge carriers in QLEDs by using the time-resolved electroluminescence (TrEL) spectra. From the TrEL spectra measurements, green and red emissions were obtained first in the QLEDs with the EMLs sequences of G/PEIE/B/PEIE/R and B/PEIE/R/PEIE/G along the direction of light emission, respectively. While the QLEDs adopt EMLs sequences of B/PEIE/G/PEIE/R, the blue, green and red emissions were obtained nearly at the same time. The above phenomenon can be attributed to different charge carrier transmission and radiation recombination process in the EMLs due to different valence band offsets and conduction band offsets between R-, G- and B-QDs by using different sequences of EMLs. White emission with coordinates of (0. 31, 0. 31) and correlated color temperature (CCT) of 5 916 K was obtained in the QLEDs with the EMLs sequences of B/PEIE/G/PEIE/R, which can be attributed to the relative uniform emission of B-, G- and R-QDs due to the effective injection and radiation recombination of charge carriers in each of the EMLs. The above results have great significance for further understanding and improving the performance of QLEDs with M-EMLs.

Key words: white QLEDs; multiple emitting layers; TrEL spectra; charge carrier dynamics
CLC number: TN312. 8 **Document code**: A
DOI: 10. 37188/CJL. 20250196 **CSTR**: 32170. 14. CJL. 20250196

基于聚乙烯亚胺插层的多发射层白色量子点发光二极管中载流子动力学的时间分辨电致发光研究

严闪闪[1], 王 申[1], 梁文城[1], 刘卫卫[2*], 孔佑超[2*]

(1.衢州学院 化学与材料工程学院, 浙江 衢州 324000;
2.盐城师范学院 物理与电子工程学院, 江苏 盐城 224002)

摘要: 量子点发光二极管(QLEDs)中,基于多发射层(M-EMLs)的载流子传输与复合动力学对器件性能具有

收稿日期: 2025-08-05; **修订日期**: 2025-08-12
基金项目: 浙江省自然科学基金联合基金(LZY24H160001); 衢州学院科研启动基金(KYQD006222001); 盐城市科技计划项目(YCBK202217); 江苏省自然科学基金(BK20241975); 盐城市政策导向性规划(YCGH007)
Supported by Joint Funds of the Zhejiang Provincial Natural Science Foundation of China (LZY24H160001); Research Startup Foundation of Quzhou University (KYQD006222001); Yancheng Science and Technology Planning Project (YCBK202217); Natural Science Foundation of Jiangsu Province (BK20241975); Yancheng Municipal Policy-guided Plan (YCGH007)

重要影响。本研究采用不同蓝(B)、绿(G)、红(R)量子点堆叠顺序的多发射层结构,并通过聚乙烯亚胺(PEIE)中间层进行分隔,利用时间分辨电致发光(TrEL)光谱直观探究了QLEDs中载流子的注入、传输及复合过程。TrEL光谱测试表明,在发光方向上具有G/PEIE/B/PEIE/R和B/PEIE/R/PEIE/G发射层序列的器件中,绿光与红光分别率先出现;而采用B/PEIE/G/PEIE/R堆叠结构的器件则几乎同时产生蓝、绿、红三色发光。这种现象归因于不同堆叠顺序下R-、G-、B-量子点间价带与导带偏移量的差异,导致各发射层内载流子传输与辐射复合过程存在差异。其中,B/PEIE/G/PEIE/R结构的QLEDs获得了色坐标(0.31,0.31)和5 916 K相关色温(CCT)的白光发射,归因于各发射层中载流子的有效注入与辐射复合使三色量子点发光相对均衡。上述发现对深入理解并优化多发射层QLEDs的性能具有重要意义。

关 键 词:白色量子点发光二极管;多发射层;时间分辨电致发光光谱;载流子动力学

1 Introduction

Modern optoelectronics demand advanced illumination systems with high efficiency and multifunctionality[1-2]. Quantum dots (QDs), as solution-processed semiconductor nanocrystals, offer narrow emission, tunable bandgaps, high quantum yield, and low-cost processing[3-5], making QLEDs ideal for next-generation displays and solid-state lighting[6-7]. Recent progress in QLEDs stems from optimized QD materials, transport layers, and device architectures[8-10]. State-of-the-art monochromatic QLEDs with sandwiched QD emissive layers (EMLs) achieve external quantum efficiencies (EQEs) exceeding 20% across red (R-), green (G-), and blue (B-) devices[11-13], highlighting superior carrier injection and suppressed non-radiative recombination.

The transition from monochromatic to white-light-emitting diodes stems from demands for natural illumination and enhanced optoelectronic efficacy[14-15]. Despite efficiency advances in white quantum dot LEDs (WQLEDs), research predominantly prioritizes device structure and electroluminescent (EL) performance[16-17], leaving operational mechanisms underexplored. Unlike monochromatic QLEDs, where EL arises from direct charge injection into QDs, WQLEDs exhibit greater complexity. Two dominant configurations exist: (ⅰ) blended EMLs containing R-/G-/B-QDs or (ⅱ) vertically stacked multiple EMLs[18-19]. Both suffer from detrimental energy transfer (ET), exacerbated by size variations in mixed monolayers[20-21] and interfacial carrier imbalances in stacked structures[22]. Physical isolation of emissive layers *via* buffer materials such as poly (p-phenylene benzobisoxazole) and metal oxides like ZnO, suppresses ET and prevents solvent damage during fabrication, though material selection requires balancing solvent resistance, electrical compatibility, and ET mitigation[23-24]. Tandem structures offer superior alternatives, with interconnecting layers inherently isolating QD-EMLs and demonstrating near-complete ET suppression *via* optimized photoluminescence[25].

However, the ET dynamics during electroluminescence and its performance impacts in white-light devices remain poorly understood. Critically, existing ET assessments predominantly rely on indirect photoluminescence (PL) methods[16,26]. Characterization approaches for monochromatic QLEDs primarily analyze device structure/material modifications and correlate them with optoelectronic responses. While effective for identifying efficiency-loss mechanisms in monochromatic devices, the absence of tailored characterization techniques for white-light devices obscures fundamental connections between monochromatic and WQLEDs physics. Conventional TrEL measurements, which detect EL intensity *via* photomultiplier tubes to probe carrier dynamics, are incompatible with color-mixed or white-light systems. Developing advanced characterization platforms specifically designed for WQLEDs is thus urgently required to elucidate their operational mechanisms and accelerate industrial deployment.

Time-resolved electroluminescence spectroscopy enables advanced characterization of carrier dynamics in QLEDs. Capitalizing on this technique, we employ wavelength-resolved TrEL to probe carrier

distributions, recombination kinetics, and electric-field-driven energy transfer in white-light devices. The solution-processable polymer polyethyleneimine, a low-work-function (3.3 eV) interlayer with demonstrated electron-injection capabilities in OLEDs, emerges as a promising interconnecting layer (ICL) candidate owing to its environmental stability and processing versatility[27-28]. Herein, PEIE-based ICLs are engineered for M-EML QLEDs to concurrently suppress Förster resonance energy transfer (FRET) and safeguard underlying emissive layers during fabrication. TrEL analysis of devices incorporating blue (459 nm), green (529 nm), and red (624 nm) QDs in varying stacking sequences reveals how valence/conduction band offsets govern carrier transport and recombination pathways. These findings correlate EML sequencing with chromaticity coordinates, enabling spectral control in multilayer architectures.

2 Experiment

2.1 Reagents and Materials

Poly (ethylenedioxythiophene): polystyrene sulphonate (PEDOT: PSS, 99.7%) and poly (9,9′-dioctylfluorene-co-bis-N, N′-(4-butylphenyl) diphenylamine) (TFB, 99.7%) were purchased from Xi'an Polymer Light Technology Corp, China. $Zn(OAc)_2 \cdot 2H_2O$ (99%), KOH (99%) were purchased from Alfa Aesar, USA. 2-Methoxyethanol (99.7%), ethanolamine (99.7%), ethanol (99.7%), and hexane (99.5%) were purchased from Aladdin, China. High-quality blue (459 nm) CdZnS@ZnS, green (529 nm) CdZnSeS@ZnS, and red (624 nm) CdSeS@ZnS QDs were purchased from Suzhou Xingshuo Nanotech Co., Ltd, China. Polyethyleneimine (80% ethoxylated, 37% (mass fraction) in H_2O) was purchased from Sigma-Aldrich. All chemicals were used without further purification.

2.2 Synthesis of ZnO nanoparticles

ZnO nanoparticles were synthesized through a sol-gel process. First, 5.488 g $Zn(OAc)_2 \cdot 2H_2O$ was dissolved in 150 mL absolute ethanol in a three-neck flask with magnetic stirring at 80 ℃ for 30 min. Separately, 2 g KOH was dissolved in 20 mL absolute ethanol with 15 min stirring. The KOH solution was added dropwise (5 min duration) to the zinc acetate precursor under vigorous stirring, followed by 5 min additional mixing. The mixture was cooled in an ice-water bath, combined with 340 mL n-hexane, and sealed for 30 min refrigeration at 4 ℃. The resulting white precipitate was centrifuged at 3 000 r/min for 5 min, washed twice with ethanol/hexane (1∶1 *v*/*v*), and vacuum-dried at 60 ℃ for 60 min. The ZnO powder was dispersed in ethanol/ethanolamine (1∶1 *v*/*v*) to prepare a 30 mg/mL colloidal solution for device fabrication.

2.3 Fabrication of WQLED Device

WQLED devices employed an ITO/PEDOT: PSS/TFB/EMLs/ZnO/Al device structure with three EMLs of B-QDs/PEIE/G-QDs/PEIE/R-QDs (denoted as D1), G-QDs/PEIE/B-QDs/PEIE/ R-QDs (denoted as D2), and B-QDs/PEIE/R-QDs/PEIE/G-QDs (denoted as D3), respectively. Indium tin oxide (ITO) glass substrates were sequentially cleaned (acetone/ethanol/water, then UV-ozone treated for 8 min. PEDOT∶PSS was spin-coated (4 000 r/min, 60 s) and annealed (120 ℃, 30 min, air) before transfer to a N_2 glovebox ($<0.1\times10^{-6}$ O_2/H_2O). TFB solution was spin-coated (8 mg/mL, 3 000 r/min, 60 s) and annealed (120 ℃, 30 min) at N_2 atmosphere. QD monolayers (R-: 3 mg/mL, G-: 2 mg/mL, B-: 8 mg/mL in n-octane) were sequentially spin-coated (2 000 r/min, 60 s) with designated stacking orders and baked (80 ℃, 30 min). PEIE interlayers (0.005 mg/mL in 2-methoxyethanol) were spin-coated (4 000 r/min, 60 s) between QD layers and annealed (120 ℃, 30 min). Non-orthogonal solvents (2-methoxyethanol/n-octane) prevented underlying layer damage during processing. ZnO NPs were then spin-coated (3 000 r/min, 60 s) before thermally evaporating the Al cathode (100 nm, 5×10^{-4} Pa). Finally, the QWLEDs were encapsulated immediately using UV-curable resin and glass covers.

2.4 Characterizations

PL spectra of B-, G-, and R-QDs were measured using an FS5 spectrofluorometer (Edinburgh Instruments) with xenon lamp excitation. Layer thicknesses in WQLEDs were characterized *via* FIB-SEM (CrossBeam, Zeiss). HRTEM and HAADF-

STEM imaging employed a high-voltage TEM instrument. Electroluminescent properties (current density, luminance, current efficiency) were measured using a Keithley 2 400 source-measure unit coupled with a Konica Minolta LS-160 luminance meter. Chromaticity coordinates were determined using an Ocean Optics Maya 2 000 spectrophotometer. TrEL measurements were performed on a system consisting of a photomultiplier tube (Zolix PMTH-S1-CR131), a digital oscilloscope (RIGOL DS4054) and a signal generator (RIGOL DG5102). The devices were driven by 400-μs rectangular pulses at 1 kHz repetition frequency.

3 Results and Discussion

The structure of D1 is shown in Fig. 1(a), comprising ITO/PEDOT: PSS/TFB/EMLs/ZnO/Al with stacked B-QDs/PEIE/G-QDs/PEIE/R-QDs EMLs. ITO and Al were used as anode and cathode, respectively. PEDOT: PSS and TFB were used as HIL and HTL, respectively. QLEDs with M-EMLs were fabricated by all-solution method. Two PEIE layers were inserted between B-, G, and R-QDs layers, respectively, which can be used to prevent the EMLs of QDs from mixing. The solvents of PEIE (2-Methoxyethanol) and QDs (octane) are non-orthogonal to each other, which can also be used to prevent the previously coated EML from damaging during the subsequent solution spin-coating process for fabrication of the following EML (Fig. S1). Fig. 1(b) displays the normalized PL spectra of the B-, G-, and R-QDs, exhibiting narrow FWHMs of 22, 21, 24 nm, respectively. Fig. 1(c) shows the molecular structure of PEIE, a low-work-function polymer critical for interfacial charge modulation. The boundaries of each functional layer are clearly revealed in the cross-sectional TEM images and element line scan (Fig. 1(d)-(e)), indicating that each layer

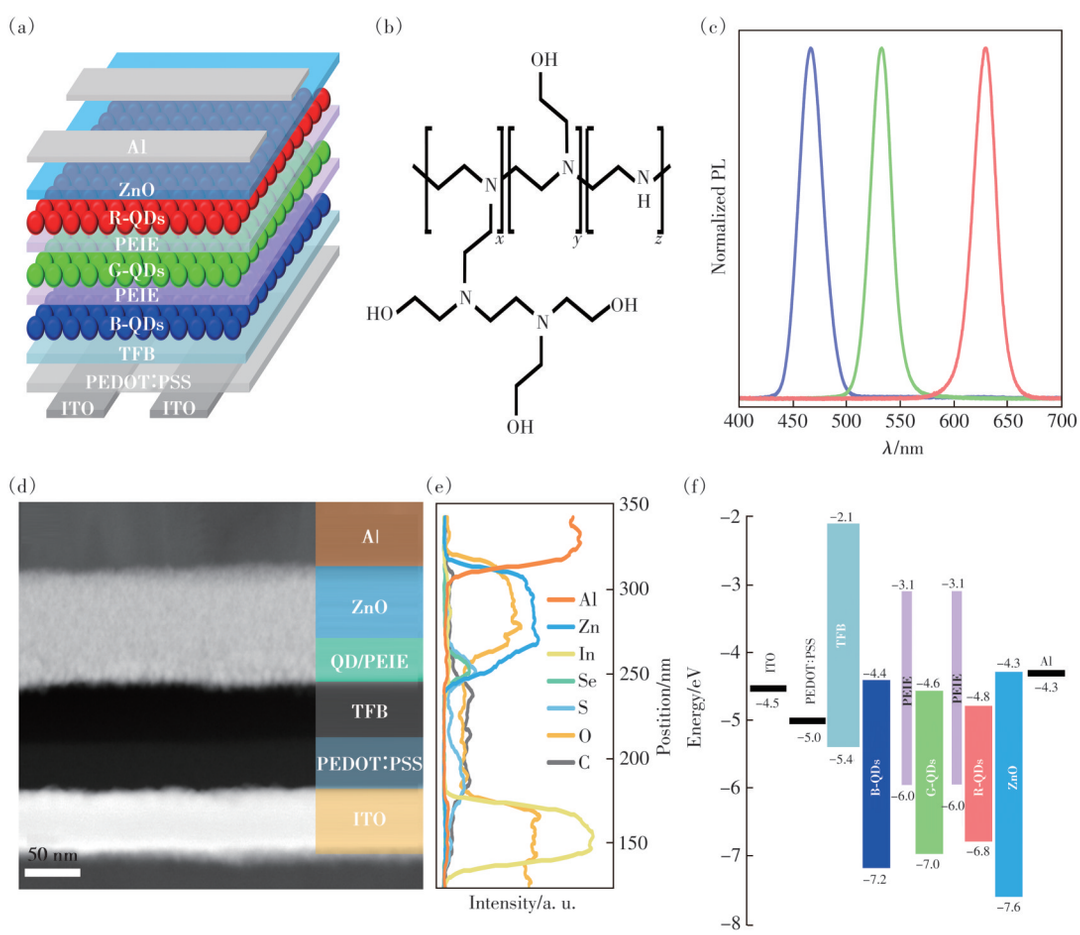

Fig.1 (a)Device architecture. (b)Molecular structure of the PEIE. (c)Normalized PL spectra of the B-, G-, and R-QDs. (d)Cross-sectional TEM image. (e)Element line scan. (f)Energy band diagram of the D1

maintains a well-defined structure throughout layer-by-layer coating process for preparing the QLEDs with M-EMLs. The thickness of each functional layer in the QLED is about 35 nm, 33 nm, 30 nm, 52 nm, and 100 nm for PEDOT:PSS, TFB, B-QDs/PEIE/G-QDs/PEIE/R-QDs, ZnO, and Al, respectively.

Due to the well-aligned conduction band energy levels between ZnO, the cathode, and the QD layer, the energy barrier for electron injection from cathode to QDs is low (Fig. 1(f)), and electrons can be injected from the cathode into the QDs layers easily. Simultaneously, ZnO's deep valence band confines holes within QD EMLs, enhancing recombination. However, significant injection barriers impede hole transport from anode through PEDOT:PSS/TFB layers. This asymmetry is compounded by higher electron mobility in ZnO *versus* hole mobility in PEDOT:PSS/TFB[29], creating charge imbalance in QD EMLs. Inserted PEIE interlayers improve charge balance by functioning as electron-blocking layers (higher conduction band than QDs/ZnO) while maintaining unimpeded hole transport. As a verification of device performance, D1 exhibits clear rectification behavior in its current density-voltage and luminance-voltage characteristics, with current density increasing under applied bias (Fig. S2). The turn-on voltage is 4.2 V, beyond which current density rises sharply. Maximum luminance of 13 640 cd/m^2 is achieved at 6 V. Peak current efficiency reaches 11.38 cd/A at 35.5 mA/cm^2. These performance metrics align closely with the reported results[30], confirming structural feasibility. While lower than state-of-the-art devices, this performance level remains suitable for investigating charge carrier injection and recombination dynamics during operation.

The EL spectra of device D1 at varying operating voltages reveal significant voltage-dependent modulation of emission intensity for the B-, G-, and R-QDs (Fig. 2(a)–(b)). Quantitative analysis (Fig. 2(c)) shows dominant B-QD emission when

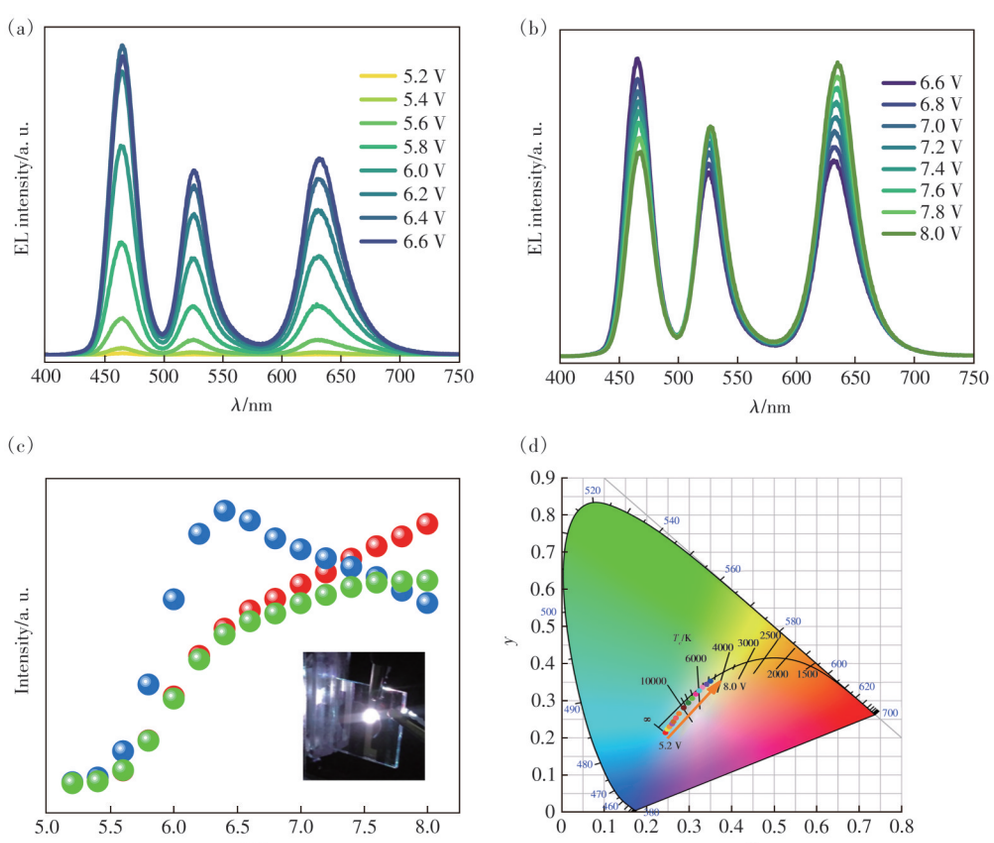

Fig.2　The EL spectra of the D1 under operation voltages of (a)5.2 V to 6.6 V and (b)6.6 V to 8.0 V. (c)The emission intensity of the individual emission peak and (d)CIE coordinates of the D1 operated at different operation voltages

the operation voltage is lower than 6.4 V, and the emission intensity increases with the applied voltage. The emission intensity of the R-QDs is nearly equal to that of the G-QDs and both show increase simultaneously with the increase of operation voltages. As mentioned before, the turn-on voltage of the WQLED is about 4.2 V (Fig. S2(a)-(b)). For thin PEIE layer and low electron injection barrier (Fig. 2(c)), the electrons are almost evenly distributed in the EMLs of the B-, G- and R-QDs when the device is turned-on. However, significant hole barriers confine exciton formation primarily to B-QDs at low voltages, explaining blue's spectral dominance. PEIE's high CBM creates intrinsic electron barriers, but operational bias enables two competing pathways: (ⅰ) trap-assisted tunneling across PEIE at low voltage, distributing carriers; and (ⅱ) voltage-enhanced trapping in low-CBM QDs (*e. g.*, R-QDs), effectively confining electrons despite high tunneling probability. This duality is resolved through carrier kinetics, where trapping rates dominate at high voltage fields. Further increasing the operation voltage, blue emission intensity decreases while red emission shows further increase and green emission tends to saturate (Fig. 2(c)). Minimal hole-injection barriers between QD layers enable rapid hole transfer from B-QDs to G/R-QDs under high electric fields, reducing exciton formation probability in B-QDs, so the intensity of the blue emission becomes weak. In addition, since the top of the valence band of the R-QDs is higher than that of the G-QDs, holes can be easily injected into the R-QDs EML after being injected into the G-QDs EML, the intensity of the red emission shows continuous increase and is higher than that of the green light, and the intensity of green emission tends to be saturated with the increase of operation voltage. With the increase of voltage from 5.2 V to 8 V, the Commission Internationale de l'Eclairage (CIE) coordinate and CCT of the QLED shifts from (0.24, 0.21) to (0.31, 0.31) and from 167 155 K to 4 794 K, respectively (Fig. 2(d) and Fig. S3). At 7.4 V, the balanced white emission with coordinate of (0.31, 0.31) and CCT of 5 916 K was obtained (inset of Fig. 4(c)), which can be attributed to the relative uniform emission from B-, G- and R-QDs. Therefore, by controlling the charge carrier transport and radiation recombination process upon operation voltage, the chromaticity parameters of the QLED can be modulated.

TrEL spectroscopy is a versatile technique to probe carrier injection/transport dynamics in EL devices, characterized by intensity evolution from initial rise to final steady-state. To investigate ET process in M-EML QLEDs, wavelength-resolved TrEL was performed on Device D1 (Fig. 3). The probe wavelength was located at 460 nm, 533 nm and 640 nm corresponding to the B-, G-, and R-QDs, respectively, slightly deviating from the emission peak to avoid the signal crosstalk due to the emission overlap. From the rising edges of the TrEL for D1 under different driving pulse voltages (Fig. 3(a)-(d) and Tab. S1), the rising time of red emission is smaller than that of green and blue emission at low driving voltage. During initial carrier injection, electrons preferentially occupy low-energy R-QD sites near the cathode due to band offset-driven trapping (Fig. 1(f)). However, high electron mobility and PEIE-enabled tunneling then facilitate redistribution across EMLs, achieving quasi-uniform steady-state distribution. This temporal resolution reconciles transient localization with steady-state uniformity. The low hole injection efficiency persists due to substantial injection barriers. However, valence band offsets (R-QDs>G-QDs>B-QDs) enable facile hole transfer from B-QDs to G/R-QDs under electric fields. Holes ultimately accumulate preferentially in R-QDs, causing the red emission first, followed by the green and blue emission (Fig. 3(a)). Above 7 V, R/G/B emissions exhibit parallel rise dynamics (Fig. 3(c)), eliminating ET as a significant factor. Elevated voltages enhance direct exciton formation in wider-bandgap QDs by promoting hole injection. Consequently, voltage dependent TrEL rise times reflect carrier redistribution dynamics rather than interlayer energy transfer.

It is well known that the EL decay after turning off the driving pulse is attributed to the existence of residual charges at the interfaces of QDs EMLs/

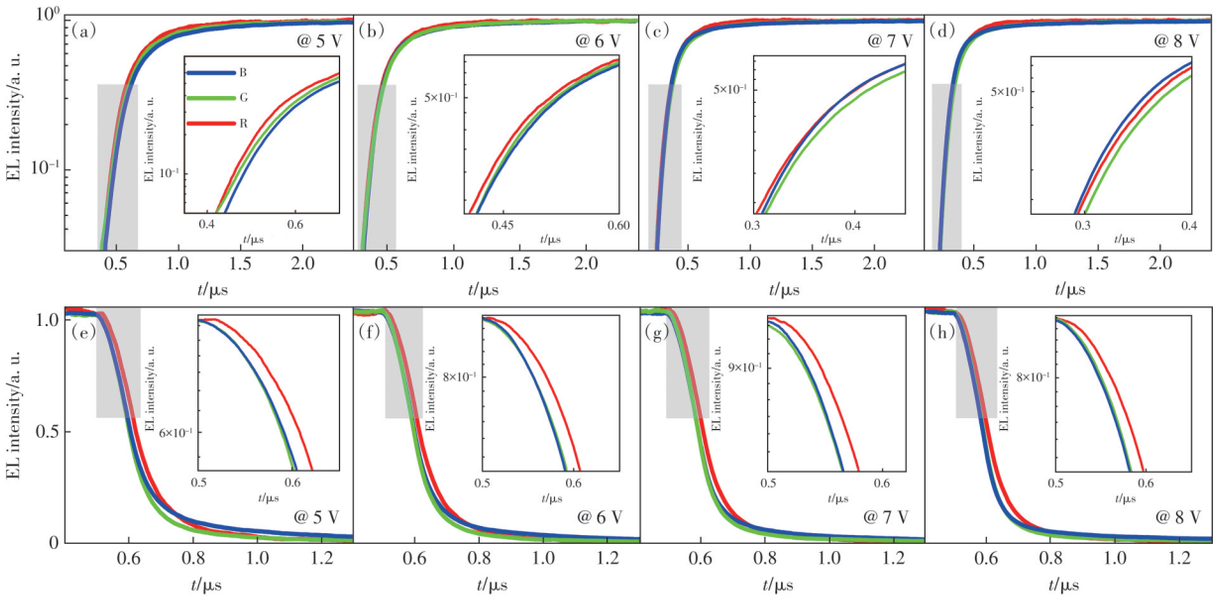

Fig.3　Normalized TrEL in the rising edges((a)-(d)) and falling edges((e)-(h)) for D1 measured at 460 nm, 533 nm and 640 nm under different voltage pulses

charge transport layers or/and in the QDs EMLs. From the falling edges of the TrEL for D1 under different driving pulse voltages (Fig. 3(e)-(h)), the decay trend is nearly the same under different driving voltages, and the decay time of the red emission is the longest. From the energy band diagram of D1 (Fig. 1(f)), the traps of electrons and holes are formed in the R-QDs layer with low conduction band and a high valence band. Compared with B-QDs and G-QDs layers, more electrons and holes remain in the R-QDs layer while turning off the driving pulse voltages, and then a longer decay time of red emission can be obtained by the radiative recombination of the residual exciton in R-QDs layer.

To compare the voltage-dependent EL spectra of different device structures, D2 and D3 with EMLs sequences of G-QDs/PEIE/B-QDs/PEIE/R-QDs and B-QDs/PEIE/R-QDs/PEIE/G-QDs were fabricated, respectively. For D2 below 6 V, the intensity of green and red emission shows obviously enhancement while blue emission remains stable with the increase of operation voltages (Fig. 4(a)). Further increasing the operation voltage, all the colors enhance until red and blue saturate at higher voltages, with green continuing to increase. D2's band structure (Fig. S4(a)) facilitates electron injection into R-QDs and tunneling to B-/G-QDs due to low barriers. Significant hole barriers initially confine holes to high-valence-band G-QDs for exciton formation and radiate recombination luminescence. At elevated

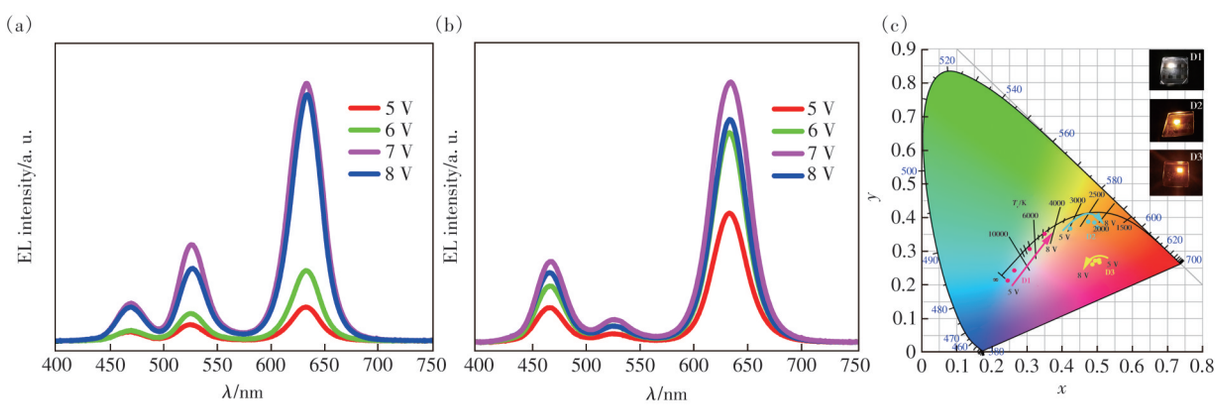

Fig.4　The EL spectra of the (a)D2 and (b)D3, and (c)CIE coordinates of the D1, D2 and D3 operated at different operation voltages from 5 V to 8 V, the insert is the EL photos of the D1, D2 and D3 operated at 7 V

voltages, holes tunnel through PEIE to B-QDs and subsequently to higher-valence-band R-QDs. This hole redistribution results in stronger green *versus* blue emission. R-QDs' low valence band traps holes, enhancing radiative recombination. As the operation voltage further increases, the number of excitons in the B-, G- and R-QDs layers will increase with the injection of large number of holes, which will enhance the EL emission intensity significantly. In the EL spectra of D3 (Fig. 4(b)), blue and red emissions increase substantially with voltage while green shows minimal enhancement. The band alignment of D3 (Fig. S4(b)) enables facile electron injection into G-QDs with subsequent transfer to R-/B-QDs, which can be attributed to the smaller injection barrier of electrons and thin PEIE layers. R-QDs' high valence band and low conduction band confine carriers, promoting exciton formation and strong red emission. During holes injection from ITO into the G-QD layer, the holes recombine with electrons in both the B-QDs and R-QDs layers successively. Additionally, holes injected from the R-QDs layer into the G-QDs layer must overcome a potential barrier. Consequently, green emission is markedly weak due to insufficient holes for exciton formation. CIE coordinates and EL images (Fig. 4(c)) confirm only D1 achieves balanced white emission at 7 V, demonstrating uniform carrier injection and recombination across EMLs. Unlike spatially fixed ZnO-buffered stacks, PEIE interlayers enable voltage-dependent hole redistribution. D1's blue-to-white CIE shift stems from progressive hole injection into G/R-QDs, contrasting the red-dominant initiation and minimal shift[23,31], highlighting PEIE's role in dynamic exciton balance.

To further analyze the charge carrier transmission and radiation recombination in D2 and D3, TrEL measurements were performed. D2's rising edges (Fig. 5(a)-(d), Tab. S2) reveal faster red/green emission onset *versus* blue, with green emission initiating first at low voltages (Fig. 5(a)). Compared with D1, the rising trend of red and green emission of the D2 is significantly faster than the corresponding blue emission. From the band alignment of D1 and D2 (Fig. 1(f) and Fig. S4(a)), the holes initially inject into D2's G-QDs layer due to lower injection barriers, confining early exciton formation to green emitters. In D2, the holes overcome barriers to penetrate B-QDs and subsequently access R-QDs through favorable valence band offsets under high pulse voltage (larger than turn-on voltage), yielding synchronous red/green rise times surpassing blue. As the pulse voltage increases above 7 V, sufficient hole injection into B-QDs accelerates blue

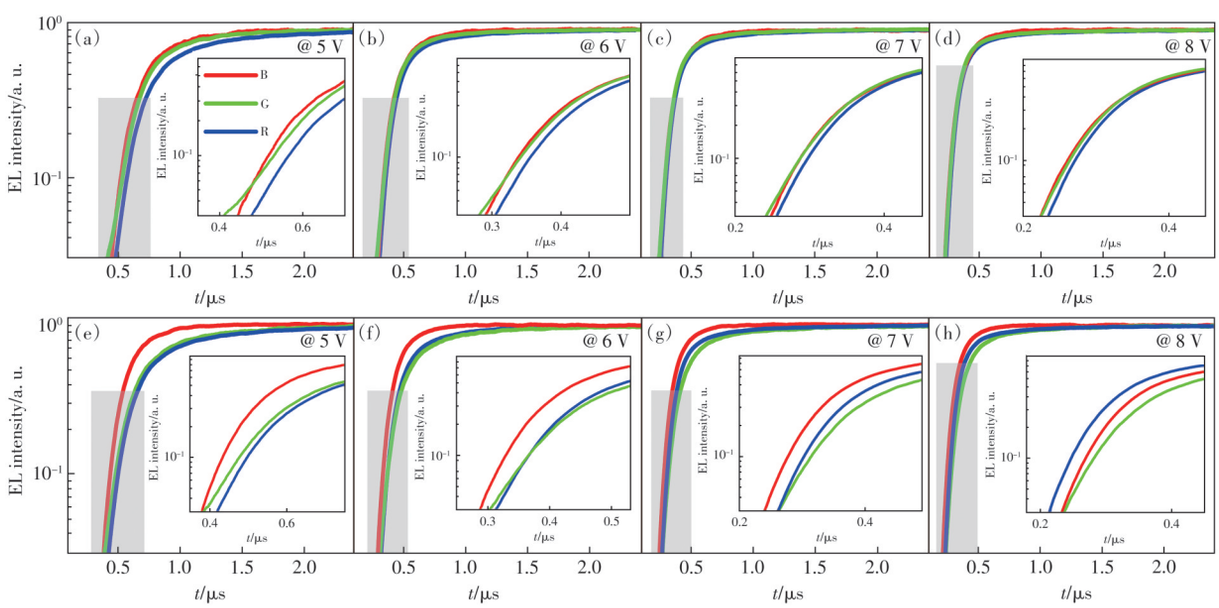

Fig.5 Normalized TrEL in the rising edges for D2((a)-(d)) and D3((e)-(h)) measured at 460 nm, 533 nm and 640 nm under different voltage pulses

emission onset (Tab. S2), narrowing rise-time disparities among colors (Fig. 5(b)-(d)). This convergence confirms absent inter-QD energy transfer between the three QDs EMLs.

In D3, red emission initiates first under low voltages (Fig. 5(e)) due to carrier confinement in R-QD traps *via* band alignment (Fig. S4(b)), enabling preferential exciton formation. Unlike D1's sequential hole injection, which are sequentially injected into the B-, G-, and R-QDs layers, and part of the holes is recombined with electrons in the B- and G-QDs layers during the process of injecting holes into the R-QDs layer. In D3, holes are directly injected from the B-QDs layer to the R-QDs layer, instead of being partially recombined in the G-QDs layer like in D1. Consequently, R-QDs accumulate more excitons, accelerating red emission rise *versus* blue/green (Tab. S1-S2). As the pulse voltage increases, both green and red emission saturate while the accumulation and recombination of excitons in the B-QDs layer become large, markedly accelerating blue emission. Above 7 V, all emissions exhibit stable rise dynamics (Fig. 5(f)-(h)), indicating sufficient hole injection. The above results are consistent with the results of the TrEL trends of D1/D2. Critically, D3 demonstrates faster red emission rise compared with D1/D2 across all voltages, reflecting higher exciton recombination probability in narrow-bandgap R-QDs *versus* wide-bandgap B/G-QDs. This recombination dominance depletes holes available for G-QDs, suppressing green emission rise kinetics. Owing to higher carrier potential in R-QDs across all device structures, electrons and holes preferentially accumulate in this layer. Consequently, red emission consistently exhibits the slowest intensity attenuation after voltage termination (Fig. S5(a)-(h), Tab. S1-S2), attributable to prolonged exciton recombination from residual carriers in R-QDs. This attenuation behavior aligns with D1's TrEL falling-edge measurements.

4 Conclusion

In summary, we demonstrated QLEDs fabricated based on M-EMLs with different stacking sequences and PEIE interlayers, where the functional layers (PEDOT:PSS, TFB, QDs, PEIE, ZnO) are processed *via* spin-coating, while the Al metal electrode is deposited by thermal evaporation. TrEL spectra were used to intuitively characterize the injection, transport and recombination of the charge carriers in QLEDs. Crucially, the synergistic combination of QD stacking sequences and PEIE interlayers modulated hole injection barriers through valence/conduction band offsets between R-/G-/B-QDs and PEIE's hole-transport facilitation. Consequently, the formation probability and spatial distribution of excitons generated by injected carriers in each EML will be altered, leading to shifts in the QLEDs' chromaticity characteristics. Balanced white emission (CIE: 0.31, 0.31; CCT: 5 916 K) was achieved exclusively in the B/PEIE/G/PEIE/R stack, attributable to uniform exciton radiation across all EMLs *via* PEIE-mediated charge redistribution. These findings hold significant implications for enhancing the performance and practicability of the QLEDs with M-EMLs, as well as other optoelectronic devices.

Supplementary Information and Response Letter are available for this paper at: http://cjl.lightpublishing.cn/thesisDetails#10.37188/CJL.20250196

References:

[1] MA T, CHEN J, CHEN Z Y, *et al.* Progress in color conversion technology for micro-LED [J]. *Adv. Mater. Technol.*, 2023, 8(1): 2200632.

[2] RYU J E, PARK S, PARK Y, *et al.* Technological breakthroughs in chip fabrication, transfer, and color conversion for high-performance micro-LED displays [J]. *Adv. Mater.*, 2023, 35(43): 2204947.

[3] WU Q Q, CAO F, YU W K, *et al.* Homogeneous ZnSeTeS quantum dots for efficient and stable pure-blue LEDs [J].

Nature, 2025, 639(8055): 633-638.

[4] YUAN T, YUAN F L, SUI L Z, *et al*. Carbon quantum dots with near-unity quantum yield bandgap emission for electroluminescent light-emitting diodes [J]. *Angew. Chem.*, 2023, 135(20): e202218568.

[5] YU Y, LIANG Y, YONG J, *et al*. Low-temperature solution-processed transparent QLED using inorganic metal oxide carrier transport layers [J]. *Adv. Funct. Mater.*, 2022, 32(3): 2106387.

[6] 黄启章, 孙思琦, 刘铭泽, 等. 面向显示应用的胶体量子点电致发光二极管: 进展与挑战 [J]. 发光学报, 2023, 44(5): 739-758.
HUANG Q Z, SUN S Q, LIU M Z, *et al*. Colloidal quantum dot electroluminescent diodes for display applications: progress and challenges [J]. *Chin. J. Lumin.*, 2023, 44(5): 739-758. (in Chinese)

[7] FAN J P, HAN C F, YANG G J, *et al*. Recent progress of quantum dots light-emitting diodes: materials, device structures, and display applications [J]. *Adv. Mater.*, 2024, 36(37): 2312948.

[8] XU Y M, DIXON G J, XIE Q, *et al*. Landau-Levich scaling for optimization of quantum dot layer morphology and thickness in quantum-dot light-emitting diodes [J]. *ACS Nano*, 2025, 19(5): 5680-5687.

[9] FANG T, WANG T T, LI X S, *et al*. Perovskite QLED with an external quantum efficiency of over 21% by modulating electronic transport [J]. *Sci. Bull.*, 2021, 66(1): 36-43.

[10] YOO J, LEE K, YANG U J, *et al*. Highly efficient printed quantum dot light-emitting diodes through ultrahigh-definition double-layer transfer printing [J]. *Nat. Photonics*, 2024, 18(10): 1105-1112.

[11] SHEN H B, GAO Q, ZHANG Y B, *et al*. Visible quantum dot light-emitting diodes with simultaneous high brightness and efficiency [J]. *Nat. Photonics*, 2019, 13(3): 192-197.

[12] NONG Y Y, YAO J S, LI J Q, *et al*. Boosting external quantum efficiency of blue perovskite QLEDs exceeding 23% by trifluoroacetate passivation and mixed hole transportation design [J]. *Adv. Mater.*, 2024, 36(27): 2402325.

[13] ZHANG D D, HUANG T Y, DUAN L. Emerging self-emissive technologies for flexible displays [J]. *Adv. Mater.*, 2020, 32(15): 1902391.

[14] 邸茵, 刘莹, 吴作用, 等. 液晶光重构显示技术的发展与应用 [J]. 液晶与显示, 2024, 39(11): 1454-1462.
DI Y, LIU Y, WU Z Y, *et al*. Development and application of liquid crystal optical rewritable display technology [J]. *Chin. J. Liq. Cryst. Disp.*, 2024, 39(11): 1454-1462. (in Chinese)

[15] XIANG H Y, WANG R, CHEN J W, *et al*. Research progress of full electroluminescent white light-emitting diodes based on a single emissive layer [J]. *Light Sci. Appl.*, 2021, 10(1): 206.

[16] CHO Y, PAK S, LI B X, *et al*. Enhanced direct white light emission efficiency in quantum dot light-emitting diodes *via* embedded ferroelectric islands structure [J]. *Adv. Funct. Mater.*, 2021, 31(41): 2104239.

[17] 阙思华, 卫黎明, 周雄图, 等. 基于混合量子点的颜色可调 QLED 器件性能及其白光应用 [J]. 发光学报, 2022, 43(4): 591-597.
QUE S H, WEI L M, ZHOU X T, *et al*. Color-tunable QLED based on mixed quantum dots and its white-light application [J]. *Chin. J. Lumin.*, 2022, 43(4): 591-597. (in Chinese)

[18] XIE Y M, LIAO L S, FUNG M K. Hybrid design of light-emitting diodes in tandem structures [J]. *Adv. Funct. Mater.*, 2025, 35(21): 2401789.

[19] LEE H, SONG S W, HWANG K M, *et al*. Hybrid white quantum dot-organic light-emitting diodes with highly stable $CIE_{x,y}$ coordinates by the introduction of n-type modulation and multi-stacked hole transporting layer [J]. *J. Mater. Chem. C*, 2021, 9(36): 12248-12254.

[20] LEE K H, HAN C Y, KANG H D, *et al*. Highly efficient, color-reproducible full-color electroluminescent devices based on red/green/blue quantum dot-mixed multilayer [J]. *ACS Nano*, 2015, 9(11): 10941-10949.

[21] HAMES B C, MORA-SERÓ I, SÁNCHEZ R S. Device performance and light characteristics stability of quantum-dot-based white-light-emitting diodes [J]. *Nano Res.*, 2018, 11(3): 1575-1588.

[22] DENG M, LI Y M, ZHANG X Y, *et al*. High-efficiency pure red $CsPbI_3$ QLEDs *via* strong electron affinity interface layer engineering [J]. *Adv. Opt. Mater.*, 2024, 12(13): 2302758.

[23] LEE K H, HAN C Y, JANG E P, *et al*. Full-color capable light-emitting diodes based on solution-processed quantum dot layer stacking [J]. *Nanoscale*, 2018, 10(14): 6300-6305.

[24] CHANG C, ZHANG Q, ZHAO W F, *et al*. Highly efficient trilayered white quantum dot light emitting diodes based on

organic buffer layers [J]. *IEEE Electron Device Lett.*, 2018, 39(11): 1692-1695.

[25] JIANG C B, ZOU J H, LIU Y, *et al.* Fully solution-processed tandem white quantum-dot light-emitting diode with an external quantum efficiency exceeding 25% [J]. *ACS Nano*, 2018, 12(6): 6040-6049.

[26] QIN Z Y, SU Q, CHEN S M. Unraveling the energy transfer mechanisms in bi-color and tri-color quantum dots: toward efficient white quantum dot light-emitting diodes [J]. *Adv. Opt. Mater.*, 2023, 11(4): 2202451.

[27] KIM J H, HAN J W, KIM S, *et al.* Cathode interfacial engineering using stearic-acid-mediated polyethylenimine ethoxylated for high-performance solution-processed organic light-emitting diodes [J]. *Chem. Eng. J.*, 2022, 427: 130890.

[28] OHISA S, KATO T, TAKAHASHI T, *et al.* Conjugated polyelectrolyte blend with polyethyleneimine ethoxylated for thickness-insensitive electron injection layers in organic light-emitting devices [J]. *ACS Appl. Mater. Interfaces*, 2018, 10(20): 17318-17326.

[29] ZHANG D D, LIU Y H, ZHU L Q. Surface engineering of ZnO nanoparticles with diethylenetriamine for efficient red quantum-dot light-emitting diodes [J]. *iScience*, 2022, 25(10): 105111.

[30] CAO F, ZHAO D W, SHEN P Y, *et al.* High-efficiency, solution-processed white quantum dot light-emitting diodes with serially stacked red/green/blue units [J]. *Adv. Opt. Mater.*, 2018, 6(20): 1800652.

[31] KIM E A, LEE J Y, HAN J S, *et al.* Facile synthesis of multicolored stacked quantum dot films for efficient white light emission [J]. *ACS Appl. Nano Mater.*, 2023, 6(13): 11455-11464.

严闪闪(1993-),男,湖北黄石人,博士,讲师,2022年于中国澳门大学获得博士学位,主要从事低维半导体光电材料与器件的研究。

E-mail: yb87810@um.edu.mo

孔佑超(1988-),男,陕西西安人,博士,副教授,2021年于中国澳门大学获得博士学位,主要从事低维半导体发光器件和第一性原理计算相关的研究。

E-mail: yb87816@um.edu.mo

刘卫卫(1981-),男,江苏淮安人,博士,教授,2011年于中国科学院长春光学精密机械与物理研究所获得博士学位,主要从事半导体和量子点发光材料与器件的研究。

E-mail: liuww@yctu.edu.cn